JOURNAL OF Materials CHEMISTRY

Synthesis and characterization of Fe–Ga mixed hydroxide powders

Jose Manuel Gallardo Amores,*[a,b] Vicente Sanchez Escribano[c] and Guido Busca[b]

[a]*Departamento de Quìmica Inorgànica, Universidad Complutense, Ciudad Universitaria, E-28040 Madrid, Spain*
[b]*Istituto di Chimica, Facoltà di Ingegneria, Università, P.le J.F. Kennedy, I-16129 Genova, Italy*
[c]*Departamento de Quìmica Inorgànica, Universidad, P[a] de la Merced, E-37008 Salamanca, Spain*

Received 4th December 1998, Accepted 3rd January 1999

Several samples of iron gallium mixed oxyhydroxides with stoichiometry $Fe_{1-x}Ga_x$ (with $x=0$, 0.10, 0.25, 0.50, 0.75, 0.90) have been synthesized by a coprecipitation method. They have been characterised from the point of view of their solid state structure by X-ray diffraction (XRD), thermogravimetry and differential thermal analyses (TG–DTA), FTIR and diffuse reflectance (DR) UV–VIS spectroscopy. After drying at 393 K, only one crystalline phase denoted as α-(Fe,Ga)OOH, is found in the samples, *i.e.* a solid solution in the whole composition range in agreement with the continuous lowering of the unit cell parameter. When Ga is added in small amounts to α-FeOOH, it tends to notably hinder α-(Fe,Ga)OOH crystallisation. The electronic spectra suggest that clustering of Fe^{3+} in dilute samples may occur. Low-temperature thermal decomposition of such mixed oxyhydroxides gives rise to corundum–hematite type solid solutions in the whole compositional range.

Introduction

α-MOOH, with diaspore or goethite structure, represents a wide family of isostructural oxyhydroxides where M can be Mn, V, Al, Fe, Cr or Ga in the +3 oxidation state. This structure is based on infinite chains of edge-shared MO_6 octahedra, linked by hydrogen bonds.[1] Accurate pH control and ageing treatments must be performed to obtain this structure in a pure state avoiding the coprecipitation of other oxyhydroxide phases (*e.g.* γ-MOOH phases) and of the trihydroxides $M(OH)_3$.[2] According to the similarities of the cationic radii, extensive isomorphous substitutions can occur and thus solid solutions can be formed.[3,4] Some of these materials find application as such, *e.g.* α-FeOOH, goethite, is used in the pigment industry.[5–7] Otherwise, these compounds are direct precursors of the respective corundum-type sesquioxides α-M_2O_3 by simple decomposition upon heating; for example, high surface area α-Al_2O_3 for heterogeneous catalysis application is obtained from α-AlOOH[8] and Fe–Cr mixed oxides can be successfully prepared by decomposing the corresponding oxyhydroxide solid solutions.[9] Fe, Cr, Al and Ga oxides, either pure or mixed, find a great number of applications, for instance, as pigments,[6,7] as heterogeneous catalysts[10,11] as precursors for the production of the respective elements (*e.g.* Ga and Al) in the metallic state[12,13] and because of their formation as corrosion products of the corresponding metals and alloys.[14] Ferric oxides display important catalytic properties in particular as oxy–dehydrogenation catalysts for *n*-butenes to butadiene[10] and for dehydrogenation of ethylbenzene to styrene.[15] Recently, Ga containing oxides have been found to display very interesting catalytic properties for dehydrogenation of alkanes to alkenes[16,17] and for aromatization reactions.[18,19]

We have undertaken a study to optimize the preparation of Fe–Ga mixed oxides as new catalysts for hydrocarbon conversions. In the present paper we report our results concerning the products of coprecipitation of trivalent iron and gallium from nearly neutral solutions. The materials obtained after drying at 393 K have been fully characterised by conventional solid state techniques.

Experimental

Powders have been prepared *via* a conventional coprecipitation method as follows. Two freshly prepared solutions were obtained by dissolving measured amounts of unhydrolyzed $Fe(NO_3)_2{\cdot}9H_2O$ and $Ga(NO_3)_3{\cdot}9H_2O$ precursor salts each in 50 ml distilled water. Both solutions were mixed into a 250 ml beaker stirring continuously and adding a concentrated aqueous solution of NH_4HCO_3 slowly to reach pH 7.5. Under these conditions Fe–Ga mixed oxyhydroxide precipitates, the colour of which depends on the Fe : Ga ratio (from red–brown to yellow). The pH was chosen as a consequence of experiments carried out at lower and higher pH, where biphasic materials were obtained in agreement with the amphoteric properties of Ga hydroxide. The resulting precipitates were aged by continuous stirring for 24 h at 343 K, filtered off, washed twice with distilled water and dried at 393 K for 24 h. Samples are denoted as $Fe_{1-x}Ga_x$ ($x=0$, 0.10, 0.25, 0.50, 0.75, 0.90). Then, a portion of each sample was ground and calcined for 3 h at 673 K. The chemical analysis, performed using a Plasma II Perkin-Elmer emission spectrometer after dissolution of the precipitates in an $HF–HNO_3$ mixture, is in very close agreement with the expected sample composition (Fe/Ga experimental atomic ratio: ∞, 8.92, 3.06, 0.97, 0.31, 0.13, 0. Expected atomic ratio: ∞, 9, 3, 1, 0.33, 0.11, 0).

XRD spectra were recorded on a Siemens D-500 diffractometer (Cu-Kα radiation, Ni filter; 35 kV, 35 mA). Unit cell parameters were calculated by a dedicated least square software program.

FTIR spectra were recorded using a Nicolet Magna 750 Fourier Transform instrument. For the region 4000–400 cm^{-1} a KBr beam splitter was used with a DTGS detector. For the FIR region (600–50 cm^{-1}) a 'solid substrate' beam splitter and a DTGS polyethylene detector were used. Pressed KBr disks (IR region) or polyethylene pressed disks (FIR region) were used.

The UV–VIS spectra were obtained with a JASCO V-570 spectrophotometer in the region 200–2500 nm using pressed disks of the samples and a polymer as a reference.

TG–DTA experiments were performed in air, with a Setaram TGA 92–12 apparatus, from room temperature to 1273 K, with a heating and cooling rate of 10 K min^{-1}.

Results and discussion

XRD

Fig. 1 compares XRD patterns of the precipitates and peak positions for all samples are summarised in Table 1. The Fe-

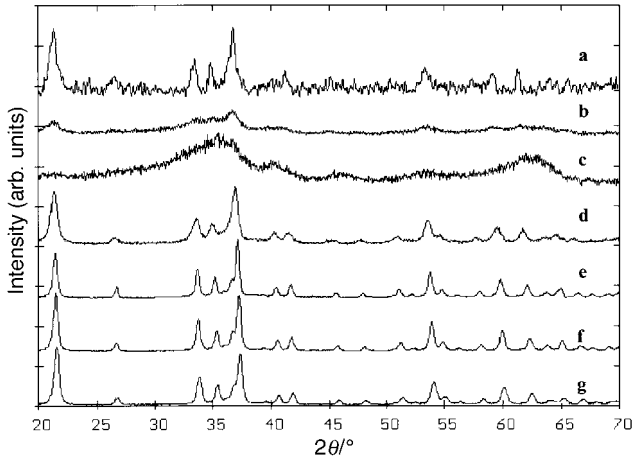

Fig. 1 XRD patterns of precipitate powders after drying at 393 K. a, Fe; b, $Fe_{1.8}Ga_{0.2}$; c, $Fe_{1.5}Ga_{0.5}$; d, $Fe_{1.0}Ga_{1.0}$; e, $Fe_{0.5}Ga_{1.5}$; f, $Fe_{0.2}Ga_{1.8}$ and g, Ga.

containing compound (Fig. 1a) is a poorly crystallised phase although peak positions and intensities agree fully with those of the oxyhydroxide goethite α-FeOOH (ICDD file no. 29–713). When gallium is present, a progressive further loss of crystallinity occurs for $Fe_{1.8}Ga_{0.2}$ and $Fe_{1.5}Ga_{0.5}$ (Fig. 1b,c). In both cases, all the peaks decrease in intensity and only major reflections can be identified. However, for $Fe_{1.0}Ga_{1.0}$ and more Ga rich samples, the same hydroxide phase is present and the samples are better crystallised. The diffraction peaks shift progressively towards lower *d*-spacing on increasing the Ga content (Table 1), resulting in a corresponding lowering of the calculated unit cell parameters and volume, as reported in Table 2. XRD peaks also increase in intensity and are progressively and continuously narrowed upon increasing the Ga content, showing a progressive improvement of crystallinity. These features must be attributed to the formation of an oxyhydroxide α-(Fe,Ga)OOH solid solution. α-GaOOH (ICDD, file no. 26–674) is isomorphous with α-FeOOH, goethite, but has smaller unit cell parameters in accord with the smaller ionic radius of octahedrally coordinated Ga^{3+} with respect to octahedrally coordinated Fe^{3+}.[1]

The Fe content into the GaOOH structure can be calculated from the unit cell parameters, according to Vegard's law.[20] The data, so calculated, agree with the theoretical Fe content obtained from the expected formula, and also with chemical analysis data which corresponds strictly to the expected values. Best agreement is found taking into account the variation of the *c* parameter.

Skeletal FTIR spectroscopy

The precipitates have been analysed by skeletal FTIR spectroscopy (Fig. 2). The Ga-free sample presents seven net absorption bands at 3126, 3050 (shoulder), 891, 796, 669 (shoulder), 627 and 454 cm^{-1} (Fig. 2a). These features are completely consistent with those of α-FeOOH as reported in the literature.[5,21–23]

Addition of Ga to FeOOH causes at first a decrease in intensity and a broadening of all spectral features (Fig. 2b,c), providing further evidence of a loss in crystallinity in agreement with the above XRD data. Further Ga addition, however, beyond a 1 : 1 Fe : Ga atomic ratio, results in the reappearance of a well resolved IR spectrum. Progressive shifts of the vibrational features are observed by further increasing the Ga content, in agreement with the formation of solid solutions.

Table 1 XRD peaks (*d*/Å) of the orthorhombic phase in precipitated mixed powders after drying at 393 K

hkl	α-FeOOH[a]	Fe	$Fe_{1.8}Ga_{0.2}$	$Fe_{1.5}Ga_{0.5}$	$Fe_{1.0}Ga_{1.0}$	$Fe_{0.5}Ga_{1.5}$	$Fe_{0.2}Ga_{1.8}$	Ga	α-GaOOH[b]
020	4.9830	5.000	4.954	4.873	4.901	4.901	4.881	4.875	4.8900
110	4.1796	4.210	4.172	4.167	4.161	4.148	4.135	4.116	4.0900
120	3.3795	3.392	—	—	3.355	3.338	3.342	3.329	3.3160
130	2.6894	2.701	2.682	2.662	2.667	2.663	2.658	2.647	2.6390
021	2.5793	2.592	2.567	2.589	2.572	2.552	2.541	2.535	2.5360
040	2.4900	2.492	—	2.461	—	2.454	2.449	2.444	2.4440
111	2.4527	2.461	2.451	—	2.435	2.424	2.415	2.409	2.4040
200	2.3030	—	2.332	—	2.334	2.290	2.288	2.279	2.2550
121	2.2528	2.260	2.273	2.246	2.238	2.229	2.223	2.217	2.2100
140	2.1915	2.195	2.219	—	2.174	2.165	2.161	2.155	2.1490
131	2.0110	—	2.024	1.999	2.003	1.987	1.984	1.979	1.9730
041	1.9200	1.932	1.918	—	1.907	1.898	1.893	1.887	1.8860
211	1.8020	1.811	1.809	—	1.792	1.788	1.782	1.775	1.7670
221	1.7210	1.724	1.718	1.734	1.711	1.705	1.701	1.695	1.6860
240	1.6940	1.697	—	1.706	1.680	1.675	1.674	1.668	1.6570
151,160	1.5640	1.568	1.552	1.525	1.552	1.547	1.542	1.539	1.5360
250,002	1.5092	1.509	1.510	1.503	1.502	1.494	1.490	1.487	1.4850
061	1.4530	1.455	1.465	1.460	1.442	1.437	1.433	1.432	1.4290

References: [a]ICDD no. 29–713 (synthetic gohetite). [b]ICDD no. 26–0674 (synthetic gallium oxyhydroxide).

Table 2 Phases and cell parameters of samples after drying at 393 K

		Cell parameters				Solubility (%Fe)[c]			
Sample	Phase	*a*/Å	*b*/Å	*c*/Å	*V*/Å^3	*a*	*b*	*c*	Expected %Fe
α-FeOOH[a]	α-FeOOH	4.608	9.956	3.0215	138.6				
Fe	α-FeOOH	4.635(8)	9.970(9)	3.022(3)	139.7	—			
$Fe_{1.8}Ga_{0.2}$	α-(Fe,Ga)OOH	4.603(15)	9.954(28)	3.029(10)	138.8	95.5	91.6	—	90
$Fe_{1.0}Ga_{1.0}$	α-(Fe,Ga)OOH	4.585(5)	9.860(13)	3.008(5)	136.0	34.2	42.1	72.5	50
$Fe_{0.5}Ga_{1.5}$	α-(Fe,Ga)OOH	4.582(2)	9.827(4)	2.987(2)	134.5	30.3	24.7	31.4	25
$Fe_{0.2}Ga_{1.8}$	α-(Fe,Ga)OOH	4.578(2)	9.804(4)	2.977(2)	133.6	25.0	12.6	11.8	10
Ga	α-GaOOH	4.559(2)	9.780(4)	2.971(2)	132.5				
GaOOH[b]	α-GaOOH	4.51	9.75	2.965	130.4				

References: [a]ICDD no. 29–713 (synthetic goethite). [b]ICDD no. 26–0674 (synthetic gallium oxyhydroxide). [c]Calculated applying Vegard's law.

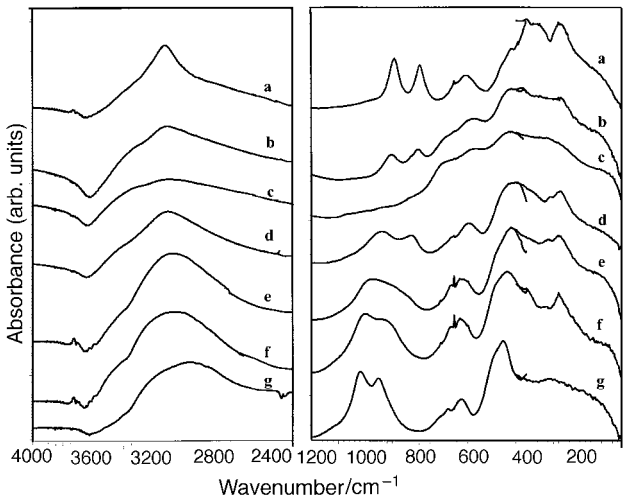

Fig. 2 FTIR spectra of precipitate powders after drying at 393 K. a, Fe; b, $Fe_{1.8}Ga_{0.2}$; c, $Fe_{1.5}Ga_{0.5}$; d, $Fe_{1.0}Ga_{1.0}$; e, $Fe_{0.5}Ga_{1.5}$; f, $Fe_{0.2}Ga_{1.8}$ and g, Ga.

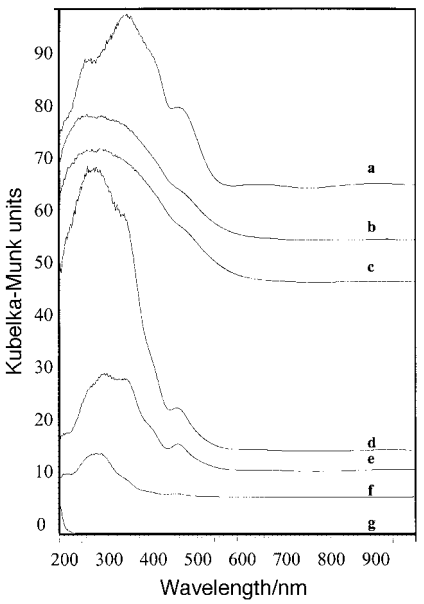

Fig. 3 Electronic spectra in the UV–VIS region of precipitate powders after drying at 393 K. a, Fe; b, $Fe_{1.8}Ga_{0.2}$; c, $Fe_{1.5}Ga_{0.5}$; d, $Fe_{1.0}Ga_{1.0}$; e, $Fe_{0.5}Ga_{1.5}$; f, $Fe_{0.2}Ga_{1.8}$ and g, Ga.

For the Ga-free sample, the band situated at 3126 cm^{-1} shifts towards lower wavenumbers down to the Fe-free compound (Fig. 2g) for which two absorption bands appear at 2913 and 2841 cm^{-1}. Conversely, the doublet found at 891, 796 cm^{-1} in the FeOOH spectrum shifts progressively upwards up to 1019, 952 cm^{-1} for GaOOH, and the main maximum at 399 cm^{-1} for goethite progressively shifts up to 486 cm^{-1} for GaOOH; the band at 627 cm^{-1} first shifts down (*ca.* 590 cm^{-1} for the sample $Fe_{1.8}Ga_{0.2}$) and later shifts up to 642 cm^{-1} for GaOOH. The spectrum of GaOOH again agrees with that reported in the literature.[24]

The goethite or diaspore structure presents an orthorhombic unit cell, in space group $Pbnm = D_{2h}^{16}$ (no. 62) with $Z = 4$. The overall unit cell and the smallest Bravais cell coincide and contain 16 atoms, thus 45 vibrational modes are expected. All atoms occupy 4c Wyckoff position in the cell on a reflection plane (C_s site symmetry). According to the correlation method[25] the determination of the number and symmetries of the optical modes has been calculated as shown in Table 3.

In agreement with previous data[24,26,27] the irreducible representation for the IR optical modes of α-MOOH is as follows, separating the modes due to the hydrogen-bonded OH groups from those of the M–O skeleton:

$$\Gamma_{MO} = 5\ B_{1u}\ (IR) + 2\ B_{2u}\ (IR) + 5\ B_{3u}\ (IR)$$

$$\Gamma_{OH} = 2\ B_{1u}\ (IR) + 1\ B_{2u}\ (IR) + 2\ B_{3u}\ (IR)$$

Consequently, the IR spectrum is expected to contain 17 fundamental modes. Clearly, we do not resolve all of them. The absorption bands near 669, 627 and 454 cm^{-1} can be related to M–O stretches of MO_6 octahedra. The features at

Table 3 Number and symmetry of the optical modes for α-MOOH structure

Symmetry	Activity[a]	M	O(I)	O(II)	H	Total	Acu[b]	Optical	M–O (sym)	O–H
A_g	R	2	2	2	2	8		8	6	2
B_{1g}	R	1	1	1	1	4		4	3	1
B_{2g}	R	2	2	2	2	8		8	6	2
B_{3g}	R	1	1	1	1	4		4	3	1
A_u	—[c]	1	1	1	1	4		4	3	1
B_{1u}	IR	2	2	2	2	8	1	7	5	2
B_{2u}	IR	1	1	1	1	4	1	3	2	1
B_{3u}	IR	2	2	2	2	8	1	7	5	2

[a]R = Raman active, IR = IR active. [b]Acoustic mode. [c]IR and Raman inactive.

Table 4 Assignments of the absorption bands in electronic spectra of precipitated powders to octahedral Fe^{3+} electronic transitions

	Electronic transition wavelength/nm						
Sample	$O^{2-} \rightarrow Fe^{3+}$	$^4A_2(^4F) \rightarrow {}^4T_1(^4P)$	$^4A_2(^4F) \rightarrow {}^4E(^4D)$	$^4A_2(^4F) \rightarrow {}^4T_2(^4D)$	$^4A_2(^4F) \rightarrow {}^4E, {}^4A_1(^4G)$	$^4A_2(^4F) \rightarrow {}^4T_2(^4G)$ or intercationic	$^4A_2(^4F) \rightarrow {}^4T_1(^4G)$
α-Fe_2O_3	257	314	375	405	444	649	885
Fe	268	*ca.* 300	362	413(s)	468	646(w)	919(w)
$Fe_{1.8}Ga_{0.2}$	263	299	—	—	475	—	930(w)
$Fe_{1.5}Ga_{0.5}$	263	305	—	—	477	—	926(w)
$Fe_{1.0}Ga_{1.0}$	263	*ca.* 300	346	416	466	687(w)	943(w)
$Fe_{0.5}Ga_{1.5}$	260(s)	300	352	402(s)	468	690(w)	960(w)
$Fe_{0.2}Ga_{1.8}$	284	—	352	405	462	—	—
Ga	—	—	—	—	—	—	—

higher wavenumbers are assigned to the in plane OH deformation modes with B_{1u} (891 cm^{-1}) and B_{2u} (796 cm^{-1}) symmetries, respectively[24,26] and to OH stretching [3125 (B_{2u}) and 3050 cm^{-1} (B_{3u})].

The shifts of the bands due to OH stretching (downwards) and in plane deformations (upwards) confirm that a progressive substitution between Ga and Fe occurs in the oxyhydroxide structure and suggest that the strengths of the hydrogen bonds between the chains of the edge shared octahedra is progressively enhanced by increasing the Ga content. This can be related to the higher electronegativity of Ga^{3+} with respect to Fe^{3+}.

Electronic spectroscopy

The electronic spectra of materials after drying at 393 K are shown in Fig. 3. The Ga-free sample (Fig. 3a) presents a

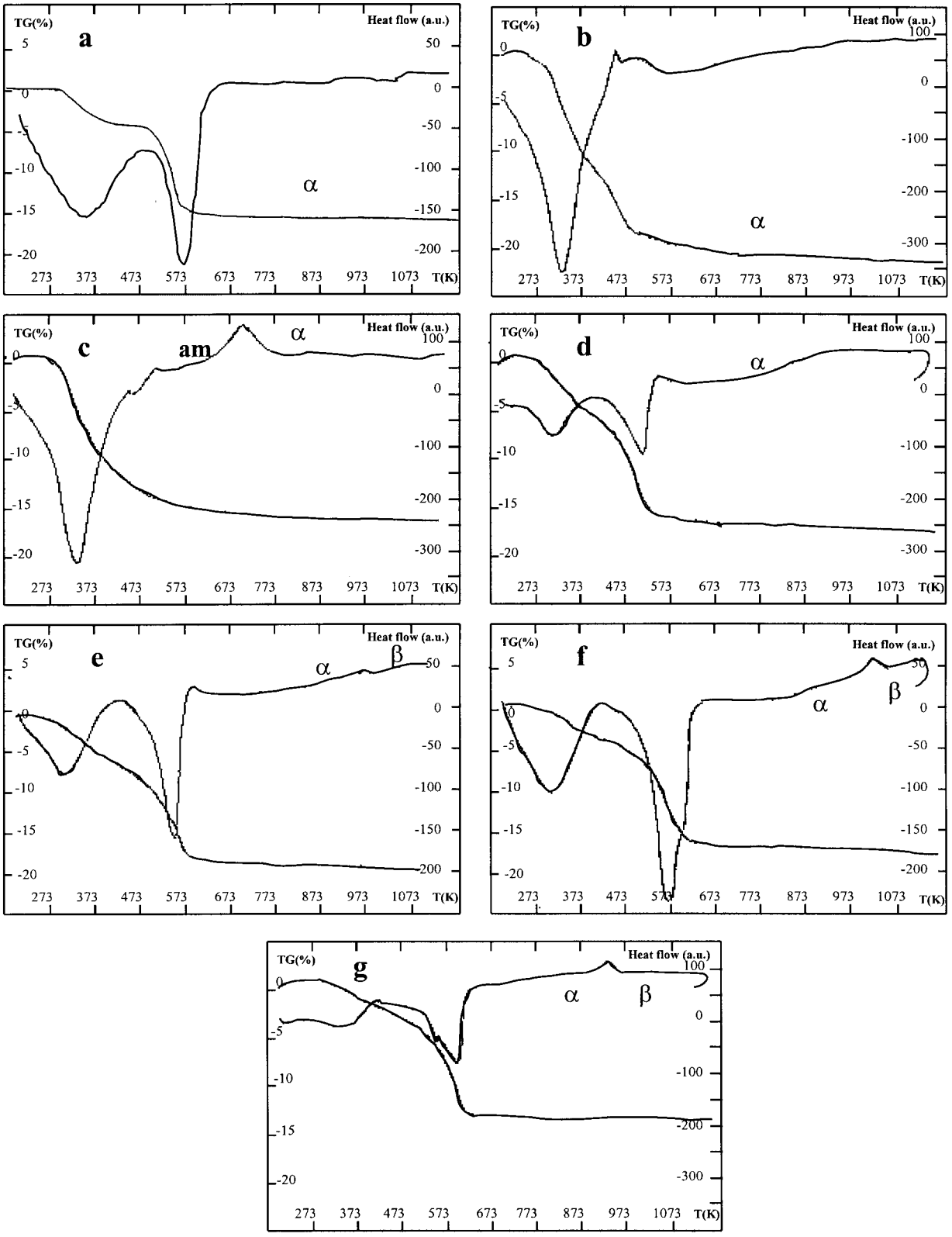

Fig. 4 Simultaneous DTA and TG curves of precipitate powders after one heating and cooling cycle. a, Fe; b, $Fe_{1.8}Ga_{0.2}$; c, $Fe_{1.5}Ga_{0.5}$; d, $Fe_{1.0}Ga_{1.0}$; e, $Fe_{0.5}Ga_{1.5}$; f, $Fe_{0.2}Ga_{1.8}$ and g, Ga.

spectrum with strong absorptions at 268, 372, and 468 nm (shoulder) and other weak features at 646 and 919 nm. This spectrum fully agrees with that reported for goethite 'yellow iron oxide' pigments.[7] The transformation of the spectrum by Ga addition reflects the modifications in oxyhydroxide structure as found by XRD and FTIR. Only one broad unresolved absorption maximum at 263 nm can be distinguished for samples with low Ga content in good agreement with the low crystallinity. A significant absorption increase is found for the $Fe_{1.0}Ga_{1.0}$ sample in agreement with its high crystallinity, while subsequently, again, the absorption tends to decrease due to the progressive dilution of Fe^{3+} by Ga^{3+}. As drawn in Fig. 3g, GaOOH does not show any absorption in the studied range except only a small increase at *ca.* 190 nm. A $O^{2-} \rightarrow Ga^{3+}$ charge transfer is expected at lower wavelengths so that the onset only of this absorption is found in the GaOOH spectrum and all features observed in the spectra of Fe-containing samples are due to Fe^{3+} ions.

A reasonable assignment of the bands in our spectra, taking as a reference the spectra of α-Fe_2O_3 reported and assigned by Lenglet and other authors[28,29] and the data of DeHaart and Blasse,[30] is summarised in Table 4. The positions of the absorptions are in accord with the octahedral coordination of Fe^{3+} in all cases. The similar positions of the absorptions detected for all samples is possibly an indication of Fe^{3+} clustering in the low Fe-content materials.

Thermal analyses

Simultaneous TG–DTA analyses were performed in air (Fig. 4). All samples show complete thermal decomposition below 673 K with weight losses of *ca.* 15–20%. Thermal decomposition of the well crystallised samples occurs in two well resolved steps at 353 and 573 K, attributed to surface water desorption and oxyhydroxide decomposition, respectively, giving rise to $(Fe,Ga)_2O_3$. The weight loss in the second step is close to the theoretical weight losses of decomposition of FeOOH (*ca.* 10%) and GaOOH (*ca.* 8.5%).

In parallel, DTA shows two endothermic peaks at 353 and 573 K, respectively, associated with the above processes.[31] Only in the case of the samples $Fe_{1.8}Ga_{0.2}$ (Fig. 4b)and $Fe_{1.5}Ga_{0.5}$ (Fig. 4c) are the two steps not resolved both in the DTA and in the TG curves, likely due again to the poor crystallinity of these samples. Instead, in the case of these samples a new weak exothermic peak is observed near 473 and 673 K, respectively, which is attributed to α-M_2O_3 crystallisation from an amorphous sesquioxide. Clearly, small amounts of Ga^{3+} hinder the crystallisation of both α-FeOOH and α-Fe_2O_3 in agreement with XRD and FTIR data. A weak exothermic feature is detected near 1100 K for the samples with Ga/Fe atomic ratio $\geqslant 3$. This peak is associated with the phase transition of the α-Ga_2O_3 type-phase to the β-Ga_2O_3 type-phase, which is the thermodynamically stable form of Ga sesquioxide.[4]

XRD study of the products of calcination of the oxyhydroxides at 673 K

Fig. 5 compares the XRD patterns of powders treated thermally at 673 K. The Ga-free sample is a well crystallised phase fully consistent with the α-Fe_2O_3 phase, hematite (ICDD, no. 33–664) (Fig. 5a). The same phase is observed in all cases, when gallium is added to α-Fe_2O_3 although the XRD peak intensity and sharpness decrease. From $Fe_{1.0}Ga_{1.0}$ the XRD pattern is again typical of well crystallised materials and *d*-spacings progressively contract upon increasing the Ga content. Finally the XRD pattern of the Ga sample corresponds to that of the α-Ga_2O_3 phase (ICDD, no. 6–503) (Fig. 5g). The calculated unit cell parameters and volumes for all samples are summarised in Table 5. These materials form a continuous corundum-type solid solution in the whole composition range

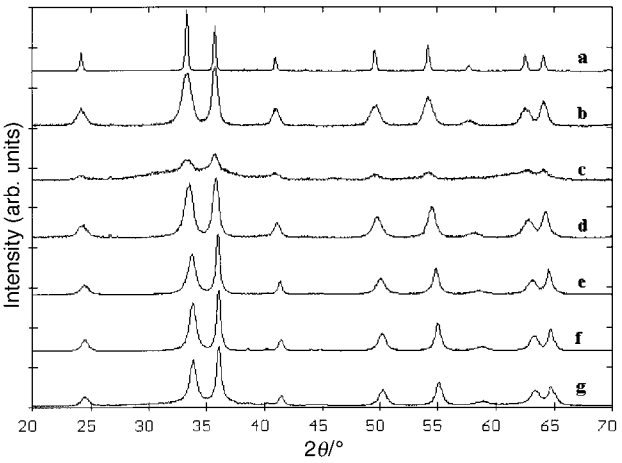

Fig. 5 XRD patterns of precipitate powders after drying at 673 K. a, Fe; b, $Fe_{1.8}Ga_{0.2}$; c, $Fe_{1.5}Ga_{0.5}$; d, $Fe_{1.0}Ga_{1.0}$; e, $Fe_{0.5}Ga_{1.5}$; f, $Fe_{0.2}Ga_{1.8}$ and g, Ga.

Table 5 Cell parameters and volumes of samples upon calcination at 673 K

		Cell parameters		
Sample	Phase	$a(=b)$/Å	c/Å	V/Å^3
α-Fe_2O_3[a]	α-Fe_2O_3	5.035	13.74	301.9
Fe		5.024(1)	13.736(3)	300.3
$Fe_{1.8}Ga_{0.2}$	α-$(Fe,Ga)_2O_3$	5.025(2)	13.731(10)	300.7
$Fe_{1.5}Ga_{0.5}$		4.993(1)	13.709(20)	295.9
$Fe_{1.0}Ga_{1.0}$		4.990(10)	13.659(21)	294.5
$Fe_{0.5}Ga_{1.5}$		4.998(4)	13.503(14)	292.2
$Fe_{0.2}Ga_{1.8}$		4.987(2)	13.475(6)	290.3
Ga	α-Ga_2O_3	4.984(0)	13.452(1)	289.4
α-Ga_2O_3[b]		4.979	13.42	288.3

[a]ICDD: no. 33–664 (synthetic hematite). [b]ICDD: no. 6–503 (synthetic α-Ga_2O_3).

with significant variations of crystallinity that reflects the crystallinity of the corresponding hydroxides. This is in accord with the well known topotacticity of the α-MOOH→α-M_2O_3 transformation.[32] The α-Fe_2O_3–α-Ga_2O_3 system resembles the α-Fe_2O_3–α-Cr_2O_3 system (where we obtained by precipitation/calcination solid solutions in the entire compositional range[9]), while it differs from those of the α-Fe_2O_3–α-Al_2O_3[33] and α-Cr_2O_3–α-Al_2O_3[34] systems, that presented only partial mutual solubility. It must however be remarked that α-Ga_2O_3 unlike α-Fe_2O_3 , α-Cr_2O_3 and α-Al_2O_3, is not thermodynamically stable but tends to convert into β-Ga_2O_3 (a defective spinel-related structure), which is thermodynamically stable.[4] On the other hand, we also note that state diagrams show that a mixed oxide phase of Fe and Ga with the formula $GaFeO_3$ exists and is thermodynamically stable near 1573 K. This phase was not found in the products of decomposition of the hydroxides described above, but can be obtained by further heating. For this reason the thermal behaviour of the α-Fe_2O_3–α-Ga_2O_3 solid solutions will be investigated further.

The possibility of formation of α-$(Fe,Ga)_2O_3$ and α-(Fe,Ga)OOH solid solutions in the entire compositional range (as found for the corresponding Fe, Cr compounds), may be due to the sufficiently similar ionic radii reported for octahedrally coordinated Fe^{3+} (0.55 Å) and Ga^{3+} (0.62 Å) (also Cr^{3+}, 0.615 Å).[1] By contrast, octahedrally coordinated Al^{3+} (ionic radius 0.50 Å). is likely too small to allow complete miscibility of the corundum-type sesquioxides.

Conclusions

The main conclusions of this study can be summarised as follows.

1 Monophasic Fe–Ga mixed hydroxides can be synthesised by a coprecipitation method based on accurate pH control.

2 These materials are goethite-type solid solutions in the whole composition range denoted as α-(Fe,Ga)OOH, where Ga progressively substitutes for Fe.

3 Low Ga contents hinder notably α-FeOOH phase crystallisation and leads to poorly crystallised materials. Conversely, α-GaOOH with small amounts of Fe retain quite high crystallinity.

4 The IR active modes related to OH stretchings and deformations show hydrogen bonding increases in strength with increasing Ga content likely due to the higher electronegativity of Ga with respect to Fe, which enhances the acidity of GaOOH groups.

5 The UV–VIS spectra are diminished upon increasing the Ga content, so showing the 'dilution' of Fe^{3+} possibly with some clustering, upon increase of Ga content.

6 These materials topotactically convert into the corresponding corundum–haematite-type solid-solution sesquioxides in the temperature range 573–773 K.

7 The crystallinity of the sesquioxides reflects the crystallinity of the oxyhydroxide precursors.

Acknowledgements

Part of this work has been supported by NATO (CRG-960316) and Junta de Castilla y León (ref.: SA37/98). J.M.G.A. acknowledges MEC for a FPI grant.

References

1 B. G. Hyde and S. Andersson, *Inorganic Crystal Structures*, Wiley Intersience, New York, 1st edn., 1989.
2 C. M. Flynn, Jr., *Chem. Rev.*, 1984, **84**, 31.
3 U. Muller, *Structural Inorganic Chemistry*, Wiley, New York, 2nd edn., 1993.
4 N. N. Greenwood and A. Earnshaw, *Chemistry of the Elements*, Pergamon Press Ltd, Oxford, 5th edn., 1995, p. 278.
5 U. Schwertmann and F. M. Cornell, *Iron Oxides in the Laboratory*, VCH, Weinheim, 1st edn., 1991.
6 *Pigment Handbook*, ed. T.C. Patton, Wiley, New York, 1988.
7 S. Ardizzone, F. Defilippi and L. Formaro, *Chim. Ind.* (*Milan*), 1985, **67**, 14.
8 R. K. Oberlander, *Aluminas for Catalysts: Their Preparations and Properties* in *Applied Industrial Catalysis*, ed. B. E. Leach, Orlando, FL, 1984, vol. 3, p. 64.
9 G. Busca, G. Ramis, M. C. Prieto and V. Sanchez-Escribano, *J. Mater. Chem.*, 1993, **3**, 665.
10 H. H. Kung and M. C. Kung, *Adv. Catal.*, 1985, **33**, 159.
11 R. J. Willey, H. Lai and J. B. Peri, *J. Catal.*, 1991, **130**, 319.
12 *Ullmanns' Encyclopedia of Industrial Chemistry*, VCH, Weinheim, 1985, vol. A12, p. 163.
13 F. E. Katrak and J. C. Agarwal, *J. Met.*, 1981, **33**, 33.
14 *Oxidation of High-temperature Intermetallic*, ed. T. Grobstein and J. Doychack, The Minerals, Metals and Materials Society, Warrendale, PA, 1988.
15 E. H. Lee, *Catal. Rev.*, 1973, **8**, 285.
16 V. Kanazirev, R. Dimitrova, G. L. Price, A. Yu Kodakov, L. M. Kustov and V. B. Kazansky, *J. Mol. Catal.*, 1990, **70**, 111.
17 R. Iezzi, A. Bartolini and F. Buonomo (Snamprogetti) IT, *Eur. Pat. Appl.*, 0 637 578 A1, 1995.
18 A. P. Singh and K. R. Reddy, *Zeolites*, 1994, **14**, 291.
19 E. Lalik, X. Liu and J. Klinowski, *J. Phys. Chem.*, 1992, **96**, 805.
20 A. R. West, *Solid State Chemistry and its Applications*, New York, 1st edn., 1989.
21 N. A. Hakeem, A. B. Basily, N. Sagr and M. A. Moharram, *J. Mater. Sci. Lett.*, 1986, **5**, 4.
22 G. Busca, N. Cotena and P. F. Rossi, *Mater. Chem.*, 1978, **3**, 271.
23 R. C. Machenzie, in *Soils Components*, *vol. 2 Inorganic Components*, ed. W. Geiseking, Springer-Verlag, Berlin, 1975.
24 A. Cornelis-Benoit, *Spectrochim. Acta*, 1965, **21**, 623; E. Schwarzmann and H. Sparr, *Z. Naturforsch.*, *Teil B*, 1969, **24**, 8.
25 W. G. Fateley, F. R. Dollish, N. T. McDevitt and F. F. Bentley, *Infrared and Raman Selection Rules for Molecular and Lattice Vibrations: The Correlation Method*, Wiley Intersience, New York 1972.
26 M. C. Stegmann, D. Vivien and C. Mazieres, *Spectrochim. Acta*, *Part A*, 1972, **29**, 1653.
27 P. G. Hall, N. S. Clarke and S. C. P. Maynard, *J. Phys. Chem.*, 1995, **99**, 5666.
28 M. Lenglet, M. Bizi and C. K. Jorgensen, *J. Solid State Chem.*, 1990, **86**, 82.
29 D. M. Sherman and T. O. Burns, *Am. Mineral.*, 1985, **70**, 1262.
30 L. G. J. DeHaart and G. Blasse, *J. Electrochem. Soc.*, 1985, **132**, 2933.
31 H. Naono and R. Fujiwara, *J. Colloid Interface Sci.*, 1980, **73**, 415.
32 P. H. Duvigneaud and R. Derie, *J. Solid State Chem.*, 1980, **34**, 23; A. L. Mackay, *4th Symposium on the Reactiviy of Solids*, Elsevier, Amsterdam, 1961, p. 571.
33 M. C. Prieto, J. M. Gallardo-Amores, V. Sanchez-Escribano and G. Busca, *J. Mater. Chem.*, 1994, **4**, 1123; V. Sanchez-Escribano, J. M. Gallardo-Amores, E. Finocchio, M. Daturi and G. Busca, *J. Mater. Chem.*, 1995, **5**, 1943.
34 J. M. Gallardo-Amores, M. C. Prieto, V. Sanchez-Escribano, C. Cristiani, M. Trombetta and G. Busca, *J. Mater. Chem.*, 1997, **7**, 1887.

Paper 8/09478K